

Article

The Test Flight of iFTEM-I Fixed-Wing Airborne Time-Domain Electromagnetic System in Binxian, Heilongjiang Province, China

Hongshan Zheng^{1,2}, Junfeng Li^{1,2}, Wei Huang^{1,2}, Yu Liu^{1,2}, Fei Li^{1,2}, Qingmin Meng^{1,2}, Qingquan Zhi^{1,2}, Xingchun Wang^{1,2}  and Ning Lu^{1,2,*} 

¹ Institute of Geophysical and Geochemical Exploration (IGGE), Chinese Academy of Geological Sciences (CAGS), China Geological Survey (CGS), Langfang 065000, China; zhongshan@mail.cgs.gov.cn (H.Z.); ljunfeng@mail.cgs.gov.cn (J.L.); huangwei@mail.cgs.gov.cn (W.H.); yuliu@mail.cgs.gov.cn (Y.L.); lfei@mail.cgs.gov.cn (F.L.); mqingmin@mail.cgs.gov.cn (Q.M.); zqingquan@mail.cgs.gov.cn (Q.Z.); wxingchun@mail.cgs.gov.cn (X.W.)

² Key Laboratory of Geophysical Electromagnetic Probing Technologies, Ministry of Natural Resources (MNR), Langfang 065000, China

* Correspondence: luning@mail.cgs.gov.cn

Abstract: The fixed-wing time-domain airborne electromagnetic method (FTEM) has been widely used in metal mining exploration, groundwater mapping and other fields worldwide, and in recent decades, its use has gradually also become more prevalent in China. The first generation of the fixed-wing time-domain airborne electromagnetic system (iFTEM-I), researched and developed by the Institute of Geophysical and Geochemical Exploration (IGGE), has been demonstrated in recent years. In this article, we introduce the brief working principle and system parameters of iFTEM-I, and we show that the effective prospecting depth of iFTEM-I is up to 350 m, which is indicated by a comparison of the results between iFTEM-I and a ground TEM system (TEM-30B) carried out in Binxian.

Keywords: iFTEM-I; Binxian; noise level; TEM-30B



Citation: Zheng, H.; Li, J.; Huang, W.; Liu, Y.; Li, F.; Meng, Q.; Zhi, Q.; Wang, X.; Lu, N. The Test Flight of iFTEM-I Fixed-Wing Airborne Time-Domain Electromagnetic System in Binxian, Heilongjiang Province, China. *Minerals* **2022**, *12*, 890. <https://doi.org/10.3390/min12070890>

Academic Editors: Guoqiang Xue, Nannan Zhou, Weiying Chen, Haiyan Yang and Behnam Sadeghi

Received: 25 April 2022

Accepted: 12 July 2022

Published: 15 July 2022

Publisher's Note: MDPI stays neutral with regard to jurisdictional claims in published maps and institutional affiliations.



Copyright: © 2022 by the authors. Licensee MDPI, Basel, Switzerland. This article is an open access article distributed under the terms and conditions of the Creative Commons Attribution (CC BY) license (<https://creativecommons.org/licenses/by/4.0/>).

1. Introduction

The fixed-wing time-domain airborne electromagnetic method (FTEM) is a geophysical exploration technique [1] which is based on fixed-wing aircraft and equipped with time-domain electromagnetic exploration equipment. INPUT (Induced Pulse Transient) was first introduced in 1959; it was the first time-domain airborne EM system which used semi-sinusoid waves with positive and reverse alternations as transmitter currents and measured the secondary field during the off-time [2,3]. This type of system can be called a pulse system. Few people appreciated the full impact that this development would have on the future of FTEM at that time [3], and in the 50 years after its first introduction, more than 20 FTEM systems (Figure 1) have been developed worldwide, such as QUESTEM, SALTMAP, TEMPEST, SPECTREM, GEOTEM, and MEGTEM [2–15]. These FTEM systems were gradually improved and developed on the basis of the INPUT system or inspired or influenced by its technical principles. They all inherited technical characteristics, except for the SPECTREM system and SALTMAP system.

PROSPECT I was first introduced in 1982, and it was upgraded and modified by the Anglo American Corp, mounted on a DC-3 turbine engine like the SPECTREM system in 1989, and then upgraded to the SPECTREM 2000 system in 1999 [3,7]. The SALTMAP project commenced in 1990 and provided a powerful new tool for land and water resource authorities [11]. Unlike the INPUT system, these two systems employed positive and reverse alternating square waves, transmitters with continuous power supplies, and no off-time, that is, measurements were carried out simultaneously in the presence of the primary field, which means they can be called full-time systems (100 duty cycle systems or on-time systems) [7,11].

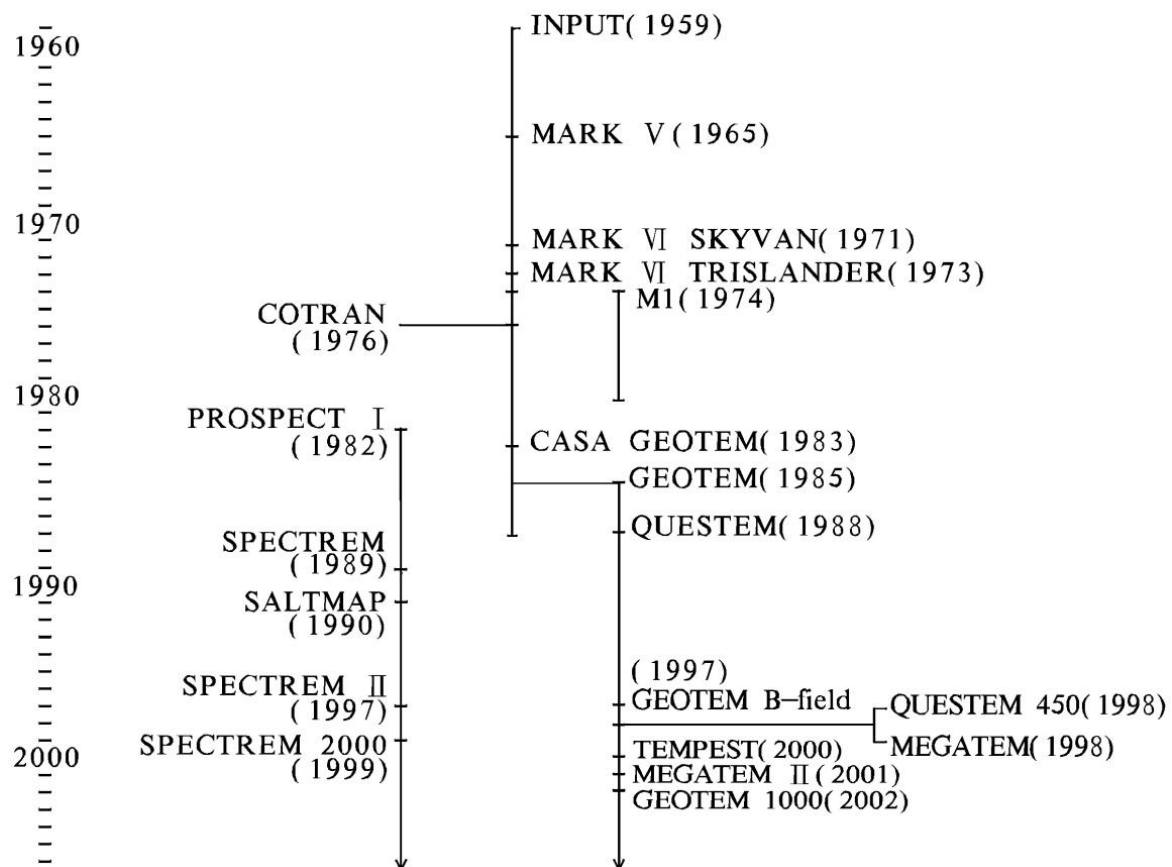


Figure 1. Overview of FTEM system development milestones from 1959 to 2006.

The R&D for airborne electromagnetic systems began in China in the late 1950s, but these systems were not developed smoothly for various reasons [15]. The former Changchun College of Geology (now Jilin University), Heilongjiang Geophysical Exploration, and Hubei Geophysical Exploration jointly developed the time-domain pulsed airborne electromagnetic system (M-1) in 1974–1980, which was installed on a Y5 aircraft and tested successfully [13]. The fundamental frequency of the M-1 was 138.9 Hz, the peak transmitter dipole moment was 59,890 Am², the sensitivity of the receiver probe was 0.66 mV/nT, and the data were received in six channels from 1.0 to 3.6 ms during the off-time period. Jilin University developed and improved the M-2 system based on the M-1 system in 1981–1983, but work was forced to be suspended due to a lack of funds. After this time, the development of FTEM systems in China mostly came to a standstill [13,14].

All of the systems described above are fixed-wing towed-bird systems. With the gradual practicability of many advanced technologies, such as computers, full digital receivers, differential GPS navigation, and so on [9,16], and as the dipole moment increased (the peak transmitter dipole moment was increased from 21 thousand Am² (INPUT, 1972) to 2.2 million Am² (MEGATEM II, 2001)), the detection depth and the ability to distinguish the target body of the systems increased [5], meaning the application scope of the systems could be expanded. By the early 21st century, these systems had been used to carry out millions of kilometers of surveys in Africa, North America, South America, Europe, and Australia, and their application fields had been extended from the original exploration of sulfide ore, uranium, kimberlite, geological mapping, groundwater mapping, erosion zone detection, etc.; however, the most important target was their use in mineral surveys [2,5,6,10,17–29].

Compared with the successful application of a large portion of the FTEM system internationally, time-domain surveys covered virtually none of China in the beginning of the 21st century. China has large areas of deserts, grasslands, basins, and plains, especially

in the northern and western regions, which largely remain underexplored. In those areas, fixed-wing time-domain airborne electromagnetic mineral exploration is suitable because of various advantages of the FTEM system, such as the fact that it is economical, highly efficient, has a large exploration depth, etc., but in this study, an FTEM system was not available, and it was too expensive to rent an advanced foreign FTEM system for use in exploration.

In order to facilitate national geological surveys and mineral exploration, which are urgently needed, and to fill a technical gap in this field at the same time, a new series of R&D projects regarding FTEM systems led by the IGGE have been being carried out since 2007. With the support of the National High-tech R&D Program (863 Program) during the 11th and 12th five-year plan period, the first fixed-wing time-domain airborne electromagnetic measurement system iFTEM-I with complete intellectual property rights has been successfully developed in China through the commitment of all partners. Subsequently, the first flight was carried out in Binxian; then, ground TEM measurements were carried out in the same area to evaluate the results of the flight.

A simple comparison between iFTEM and the typical GEOTEM system is shown in Table 1 [1,5,12–15,30]. The transmitter dipole moment of iFTEM-I is smaller, and the noise level is larger, which indicate that there is a lot of work, both in terms of increasing the dipole moment and reducing the noise level, that could be done to improve the performance of iFTEM.

Table 1. Comparison between iFTEM-I and GEOTEM.

Model	iFTEM-I	GEOTEM
Aircraft	Y12-IV	CASA-212
Aircraft speed (km/h)	230	400
Peak transmitter dipole moment (Am ²)	504,000	690,000
Transmitter waveform	half sine wave	half sine wave
Base frequency	12.5, 25	12.5, 25
Bandwidth	0–20	0–10
Data unit	dB/dt	dB/dt or dB
Noise level (nT/s)	13	1–2

2. The iFTEM-I System

iFTEM-I is a time-domain towed-bird transient electromagnetic system, and its working status is shown in Figure 2. The iFTEM-I system is mounted on a Y12-IV aircraft, and the transmitter loop is wound around wing tips, the nose, and the tail of the aircraft. A pulse signal with a certain waveform transmitting through the transmitter coil generates the primary field around it (on-time). Under the excitation of the primary field, the underground anomalous body is induced to produce an induced current, namely an eddy current or secondary current. The eddy current generates the secondary field around the body. Due to the passive excitation of the secondary field and the thermal loss of the induced current inside the body, the secondary field will gradually decay. The receiver bird receives the secondary field signal the whole time. Then, the electrical distribution structure and spatial form of the underground body can be inferred by analyzing the secondary field (off-time) [31].

iFTEM-I is based on the 5 ton load twin-engine Y12-IV aircraft as a platform. Four turns of transmitter coil are mounted on a set of integrated transmitting brackets. The loop area is 210 m², and the peak transmitter current is 600 A, which make the peak transmitter dipole moment of the system up to 504,000 Am².

The transmitting waveform of iFTEM-I is a semi-sinusoidal pulse. The pulse width is 4.15 ms, and the transmitter fundamental frequency is 12.5 Hz or 25 Hz, which can be

adjusted manually. Figure 3 shows a half-cycle waveform of iFTEM-I. The next half-cycle waveform has exactly the same shape but is in the opposite direction.

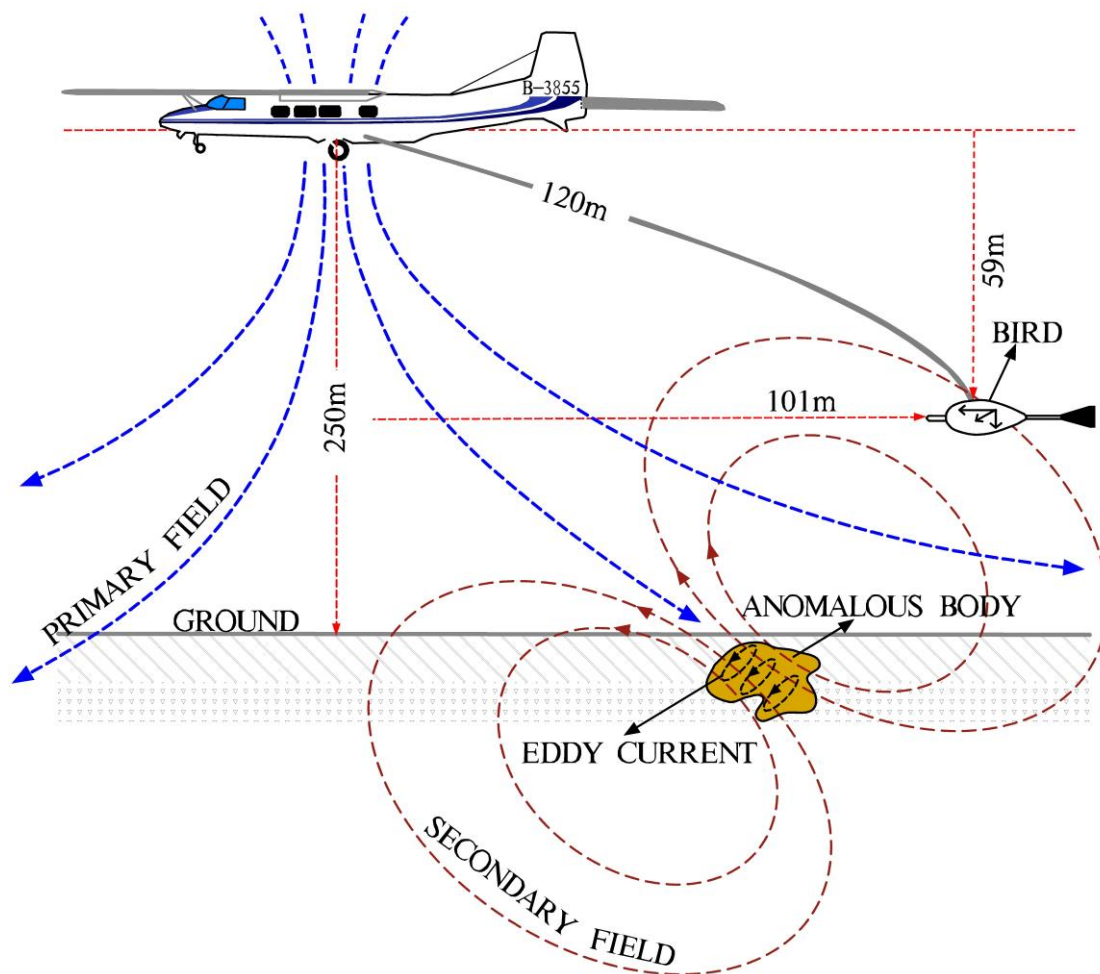


Figure 2. A schematic diagram of iFTEM-I (modified after R&D report of iFTEM-I and Reprinted with permission from Ref. [12]. Copyright 1991 Taylor & Francis).

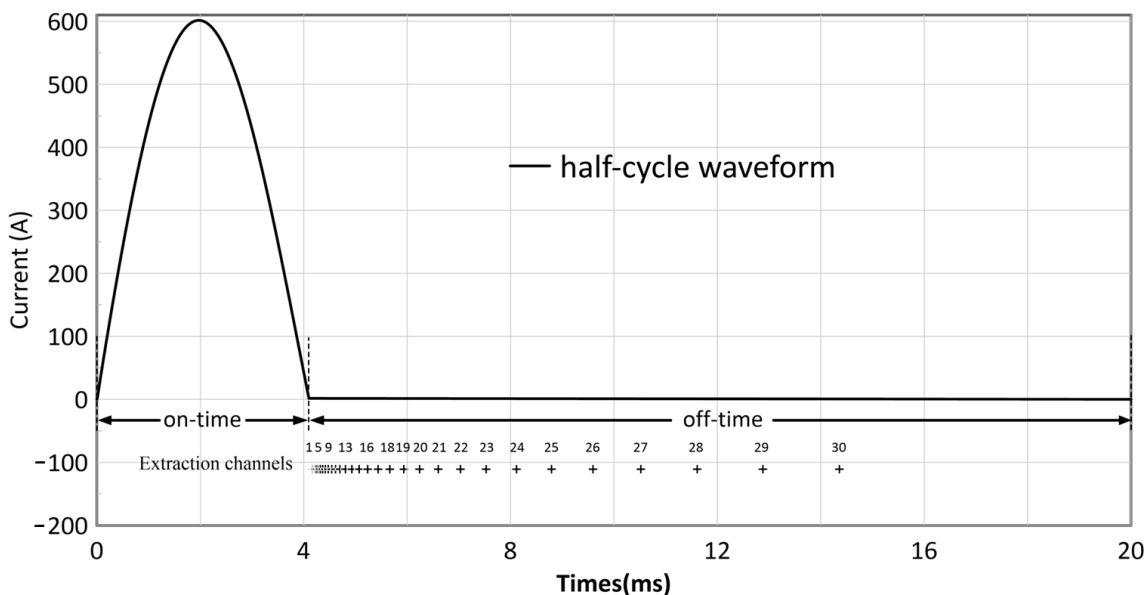


Figure 3. Half-period transmitter waveform of iFTEM-I. The plus symbols below off-time line are the gate centers of extraction windows.

The three-component receiver of iFTEM-I is installed in the receiver bird, which is mounted under the tail of the aircraft and is released and collected via a winch. The receiver bird is located 101 m behind and 59 m below the aircraft during a survey (taking the flight speed of about 230 km/h as a typical example) (Figures 2 and 4). The equivalent receiving area is 19,000 m². An acquisition system with a base frequency of 25 Hz, a sampling rate of 100 kHz, and a sampling rate of 24 bits will generate approximately 4000 rows per stack, 25 stacks per second, and 5.4 GB data per hour when recording four channels (Rz, Rx, Ry, and transmitter current Rv) synchronously.

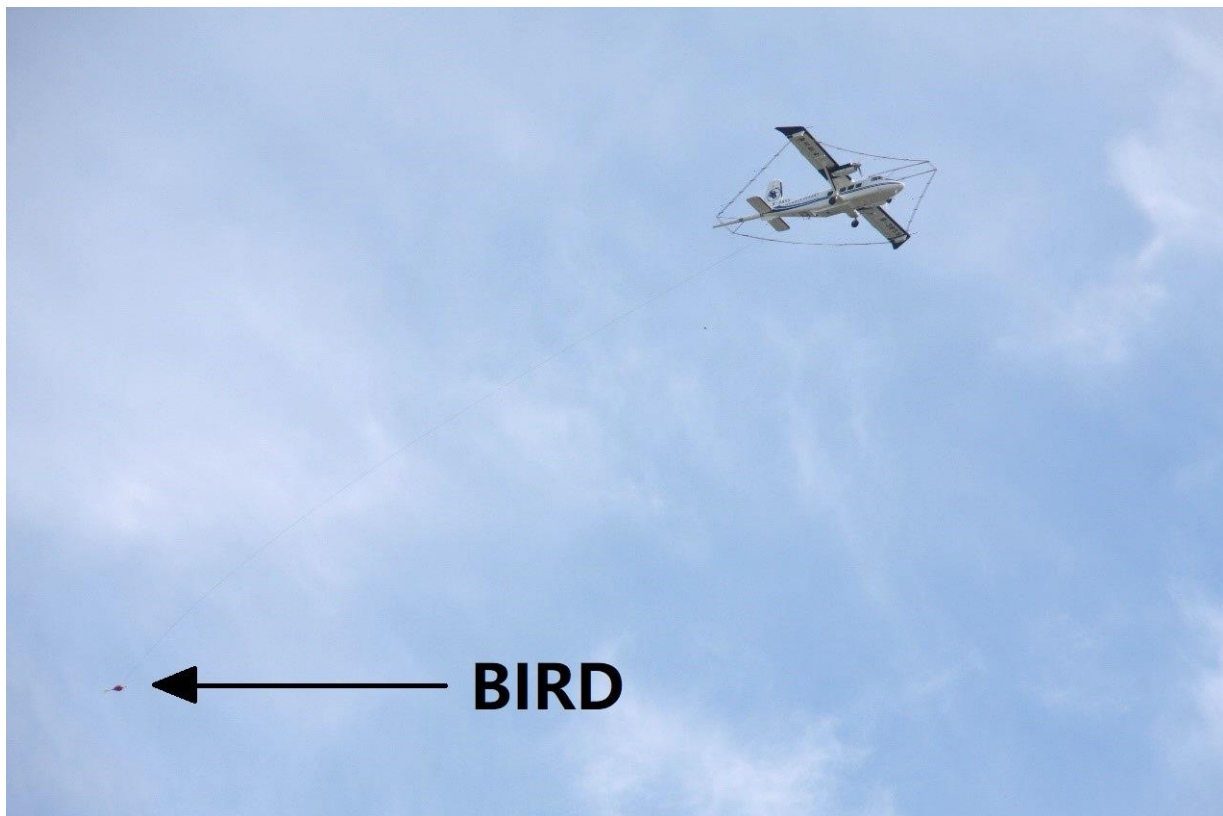


Figure 4. Overview of iFTEM-I when it is flying.

3. Survey Flight

3.1. Geological Setting

Binxian is located in the eastern part of Harbin of Heilongjiang province, about 60 km away from Harbin Pingfang airport. There are four survey lines in the survey area; the line spacing is 250 m, and the line direction is 138.9°. It can be seen from Figure 5 that the north-west (NW) parts of the survey lines are Quaternary, the middle parts are mainly reservoir, and the south-east (SE) parts are low-hilly mountains with exposed Yanshan granite. There are no drills or ores, but three hydrogeological drills are located not far from the survey area. The depths of the three hydrogeological drills are from 157 m to 204 m (Figure 6 displays the stratigraphic section of the B21 drill). The data from the drills show that the shallow surface is made up of Quaternary clay and loam with a thickness less than 30 m, and the depths below are made up of Cretaceous sandstone and mudstone. In general, the resistivity of clay, loam, sandstone, and mudstone is lower, while the resistivity of granite is higher.

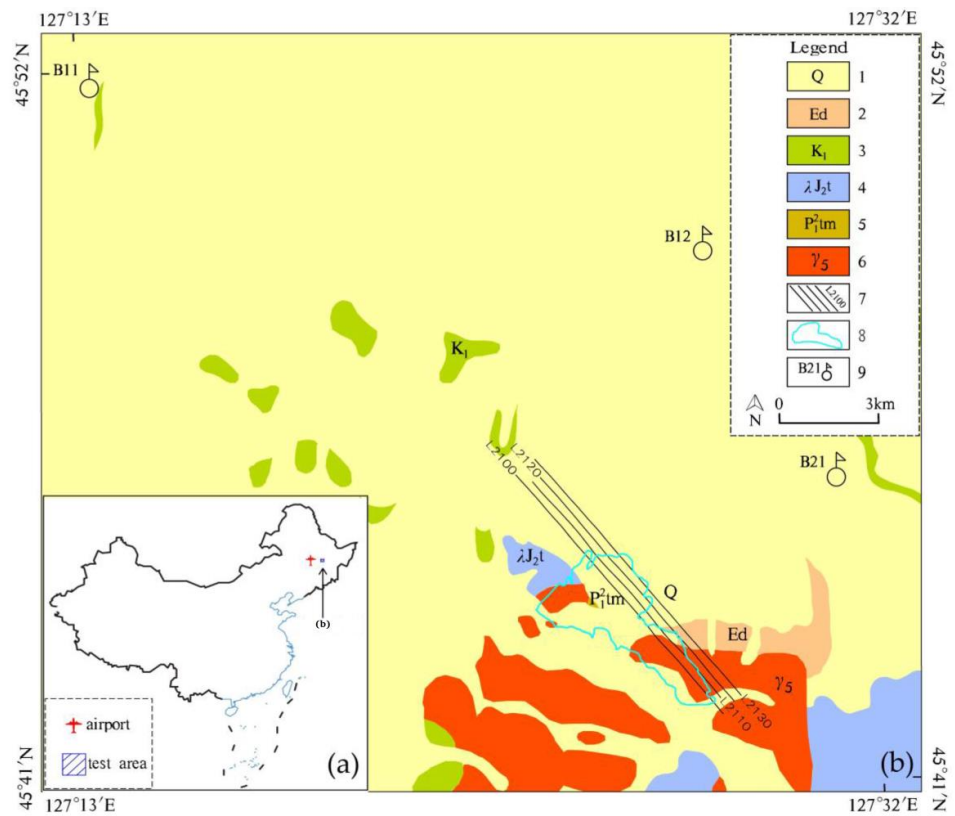


Figure 5. The overview (a) and zoom (b) of Binxian. 1—Quaternary clay and loam, 2—Paleogene sandy conglomerate and sandstone, 3—Cretaceous mudstone and sandstone, 4—Jurassic rhyolite and tuff, 5—Permian slate and sandstone, 6—Yanshanian granite, 7—flown footprint, 8—reservoir, 9—drills.

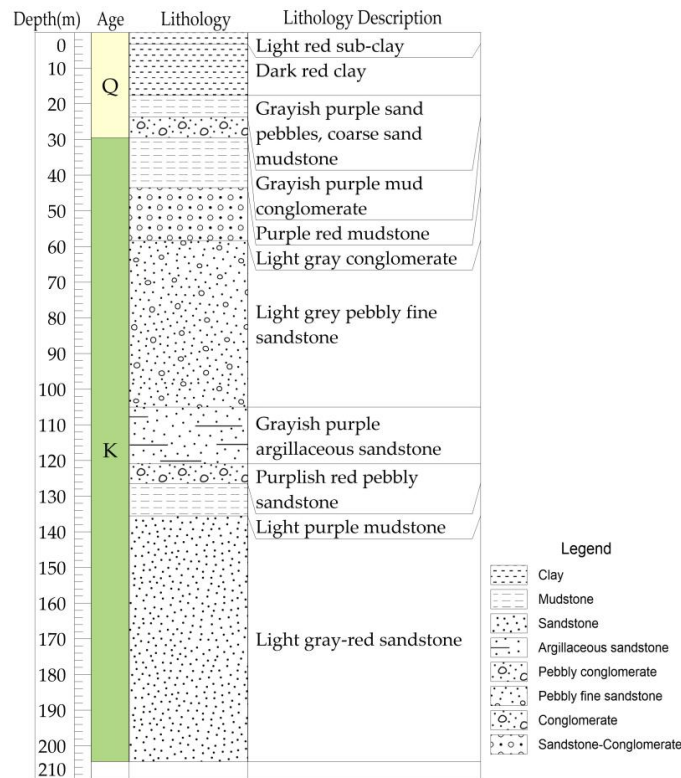


Figure 6. Stratigraphic section of Binxian B21 drill (modified after internal information).

3.2. Survey Flight and Data Processing

The survey flight was carried out on 18 July 2016. The main parameters of the iFTEM-I system are shown in Table 2. The actual flight path is shown in Figure 5. Four lines were measured in the flight, with an average flight altitude of 202.7 m.

Table 2. iFTEM-I system parameters for the test flight in Binxian.

Parameters	Values
Transmitter base frequency	25 Hz
Transmitter height (VAGL ¹)	210 m
Receiver bird height (VAGL)	151 m
Transmitter–bird horizontal separation	101 m
Transmitter peak current	600 A
Transmitter pulse width	4.15 ms
Loop area	210 m ²
Number of turns	4
Transmitter dipole moment	504,000 Am ²
Equivalent receiver area	19,000 m ²
Sampling rate	100 kHz
Sampling bits	24 bits
Data channels	Rv, Rz, Rx, Ry, Longitude, Latitude, GPS_time, GPS_Altitude, Radar_altitude
Gate centers after on-time (post data processing)	4.36, 4.38, 4.40, 4.43, 4.46, 4.49, 4.53, 4.58, 4.63, 4.70, 4.77, 4.86, 4.96, 5.08, 5.22, 5.38, 5.57, 5.79, 6.04, 6.35, 6.70, 7.12, 7.60, 8.17, 8.83, 9.60, 10.50, 11.55, 12.78, 14.22 ms

¹ VAGL represents vertical above ground level.

The measured data were stored, processed, and analyzed by using the GSS platform, which was independently developed by the IGGE. The platform not only has large data storage, efficient data access, easy function expansion, a friendly user interface, etc., but also can be used as a general support platform for the development of airborne geophysical or other application software with similar data structures [32]. In addition, some cartographic and data analyses were completed with Surfer, Grapher, Oasis Montaj, and other software. In this article, we mainly processed and analyzed the vertical component, the Z component of the data, because of the technical difficulties in the horizontal component (X, Y).

Due to the very high sampling density of iFTEM, the amount of data acquired in surveys is very large. It is unnecessary to include all these data in the subsequent data processing step, and it would take too much time. Therefore, to ensure the data quality, window data sampling of the data is carried out to reduce the amount of data. In this article, window channel sampling was carried out for data in the off-time period using software. The central times and widths of these sampling windows are shown in Figure 3, with a total of 30 sampling windows, the central times of which range from 4.36 to 14.22 ms (the 0 time starts from the on-time).

The noise level is an important index for the evaluation of the performance of measurement systems. iFTEM-I uses high–altitude flight survey (baseline) data to calculate noise levels. When the measurement system flies at a high true height, such as 1000–2000 m, the transmitter subsystem still works normally at a certain fundamental frequency and transmitter current. At this time, as the distance from the ground is high, the secondary field response generated by the geological body will be very weak. Thus, the response signal collected by the receiving subsystem not only includes the primary field generated by the aircraft metal body, industrial electricity noise, thunder, and other spatial noise, but also includes the dynamic noise generated by the receiver coil cutting the geomagnetic

field. The received response signal of the high-altitude flight measurement is statistically calculated, and the noise level of the system is obtained.

The noise level is generally calculated by using the late time channels' data after being extracted. In this article, the standard deviation method and the peak-to-peak statistical method were used to calculate the late time channels' noise level.

The formula of the standard deviation method is shown below:

$$SD_j = \sqrt{\frac{1}{2M} \sum_{i=j-M}^{j+M} (X_i - \bar{X})^2} \tag{1}$$

where \bar{X} is the average of the X_i over the range $[j - M, j + M]$. The standard deviation noise estimate SD at sample j is calculated using a window of 201 points ($M = 100$; in this case, 201 points corresponds to a width of nearly 500 m), and then, the maximum of the last three channels is about 2.7 nT/s.

The peak-to-peak statistical method was adopted to select the last three late channels' data after being preprocessed (Figure 7). The maximum difference calculated between the maximum peak value and the minimum peak value was taken as the noise level of the data. In this way, the noise level of iFTEM-I, flown in Binxian, was 13 nT/s, which was the noise level of the last three late channels' data (Figure 7b) after de-noising and correction pretreatment was applied to the measurement data of the high-altitude background field (Figure 7a).

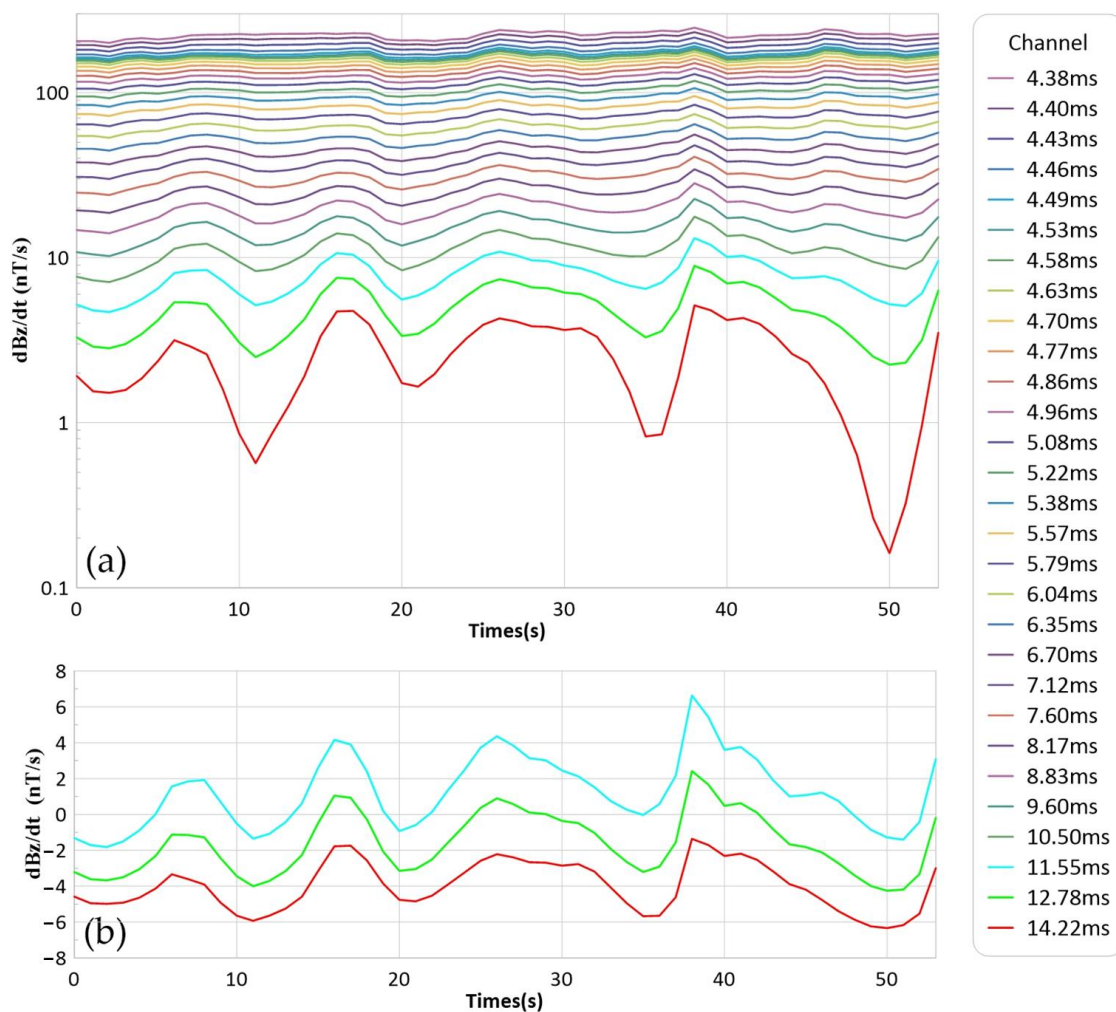


Figure 7. Noise level statistics (peak-to-peak). (a) Baseline data after pre-processing; (b) the last three late channels' data for baseline data.

In this article, the peak-to-peak statistical method was the more reasonable choice, because the data used for noise statistics were pre-processed data which were filtered to a certain extent, although the peak-to-peak noise level was higher than the standard deviation noise level.

3.3. Mapping

It is well known that the response value of the vertical component of the TEM varies with the electrical properties of underground materials. In general, high response values usually correspond to low-resistivity materials, while low values correspond to high-resistivity materials. Therefore, the electrical distribution pattern of subsurface materials can be analyzed using the variation characteristics in a planar TEM contour map. In the TEM, with the increase in transient electromagnetic sampling delay, data from early channels to late channels basically reflects geoelectric information from shallow to deep depths. A variation in delay is usually represented by a sampling channel (hereinafter abbreviated as CH). Figure 8 shows the amplitude of the response plane corresponding to CH1, CH5, CH10, and CH15 in the vertical component. It can be seen from Figure 8 that the NW section of the contour corresponds to the low-resistivity area, and the SE section corresponds to the high-resistivity area, which are consistent with the regional geological and hydrological drill data.

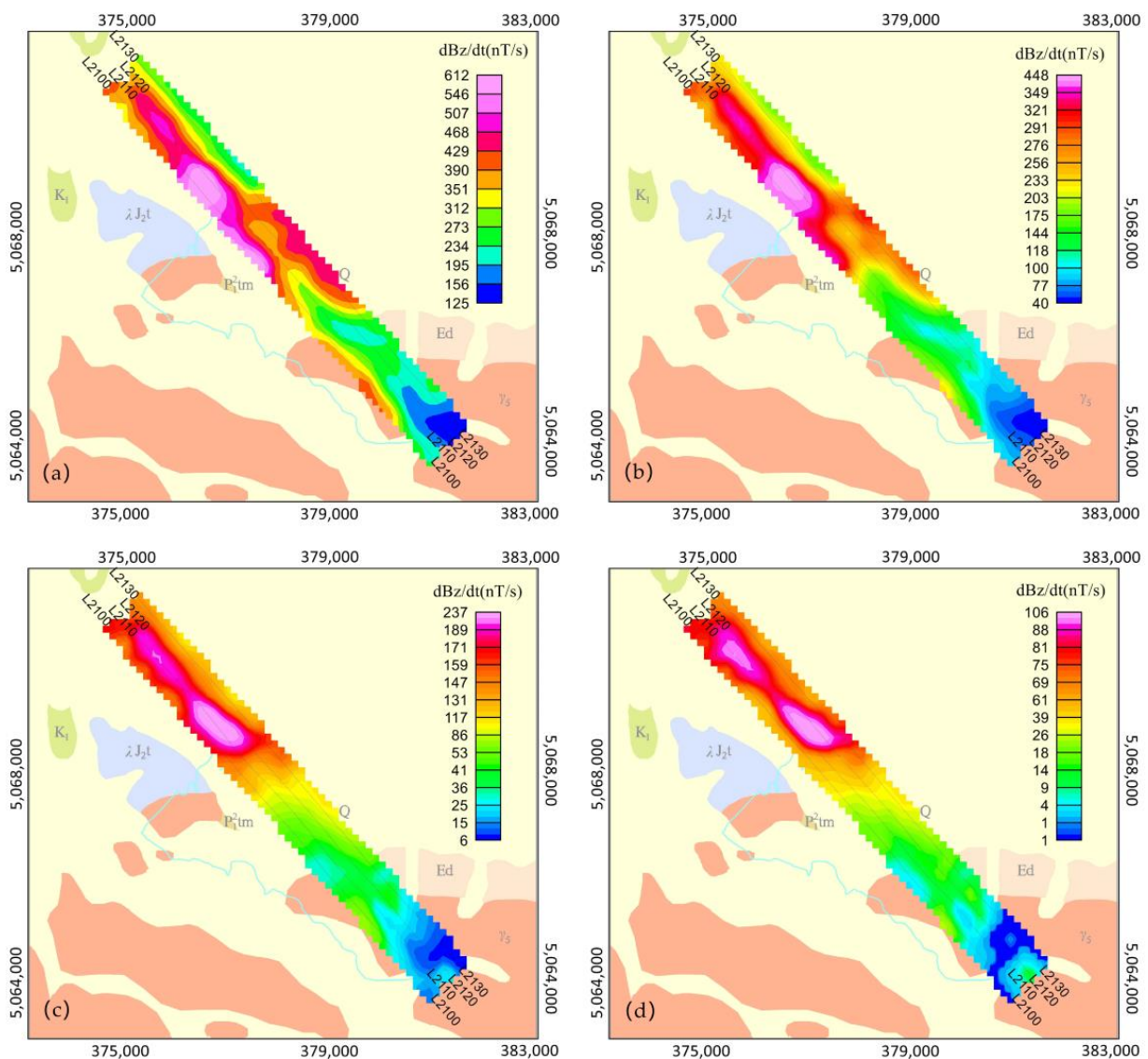


Figure 8. Contour map of $\frac{dBz}{dt}$ of 4 different sampling channels. (a) CH1; (b) CH5; (c) CH10; (d) CH15.

Maxwell’s one-dimensional aerial EM inversion module (SVD) was used to calculate the inversion of iFTEM-I data. This approach began with the uniform half-space model, and the first 22 channels of data were selected for inversion according to the noise level of the system. The results were then compared with drill and geological data, and the inversion results were examined using horizontal slices ranging from -20 to -400 m. As seen in Figure 9, the resistivity of the NW section is lower, while in the SE section, it is higher, which is consistent with the NW section’s strong response. The NW section’s resistivities are nearly constant at different depths. Given that this portion is covered by the Quaternary and that the Cretaceous and Quaternary are both shallow at -200 m, it is concluded that the Cretaceous mudstone and sandstone under the thin Quaternary clay and loam are shallow at -400 m in the NW region. While the SE section has higher resistivities, it increases with depth from 140 to around $3000 \Omega\cdot\text{m}$. Due to the fact that this portion is mostly Yanshanian granite, it could be concluded that the shallow section of the SE section is granite at -400 m.

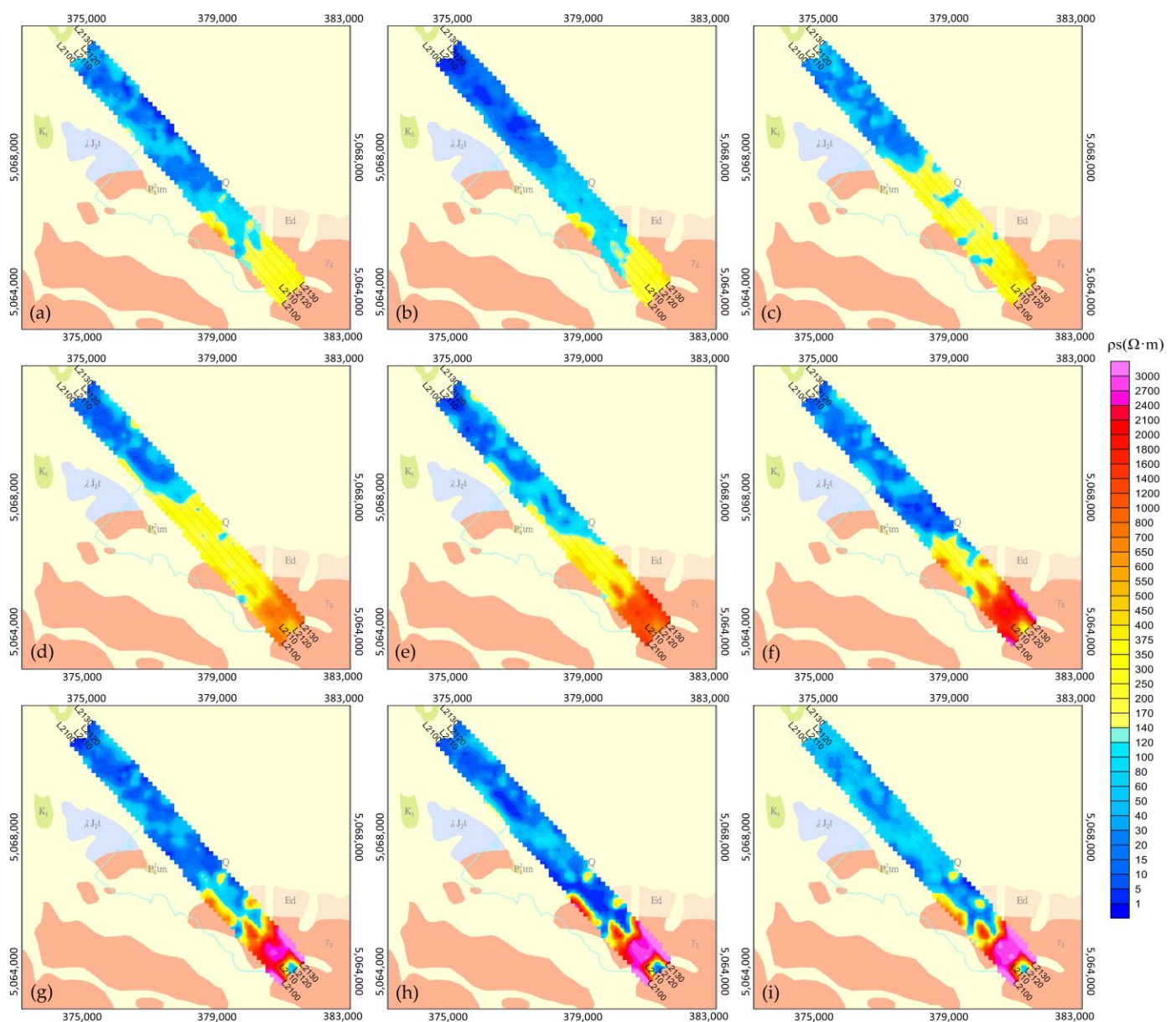


Figure 9. Resistivity plane contour map at different depths: (a) -20 m; (b) -60 m; (c) -100 m; (d) -150 m; (e) -200 m; (f) -250 m; (g) -300 m; (h) -350 m; (i) -400 m.

4. Ground TEM Survey

In order to verify the validity of the iFTEM data in the survey area, ground TEM measurements were carried out on the same survey lines. According to the field survey, electromagnetic interference was found in the NW section of the survey line, from things such as human buildings, iron fences, highways, and high-voltage power lines. In the middle section of the survey lines, there was electromagnetic interference from things such as human buildings, an iron fence around the reservoir, etc. Additionally, the electromagnetic interference in the SE section of the survey lines mainly came from the iron guardrail of the reservoir and the cemetery. All of these electromagnetic interferences had significant adverse effects on both the ground and airborne TEM data. In contrast, the central location of the reservoir had relatively lower electromagnetic interference as it was further away from human buildings. Therefore, the ground TEM survey was carried out on the L2100 line when the ice was thick and safe enough in the winter of 2018. The measured point locations are shown in Figure 10. Ground TEM data were acquired using TEM-30B, which was developed by the IGGE. The parameters of TEM-30B were as follows: the size of the transmitter coil frame was 100 m × 100 m, the pulse width was 40 ms, the base frequency was 12.5 Hz, the ramp was 70 μ s, the transmitter current was 6.3 A, and the stacking times were generally 512, which were increased to 1024 or higher in the area with large interference according to the actual situation. The overlapped loop was used to receive data in 47 channels after on-time, and the gate centers were over the range [0.015 ms, 33.855 ms].

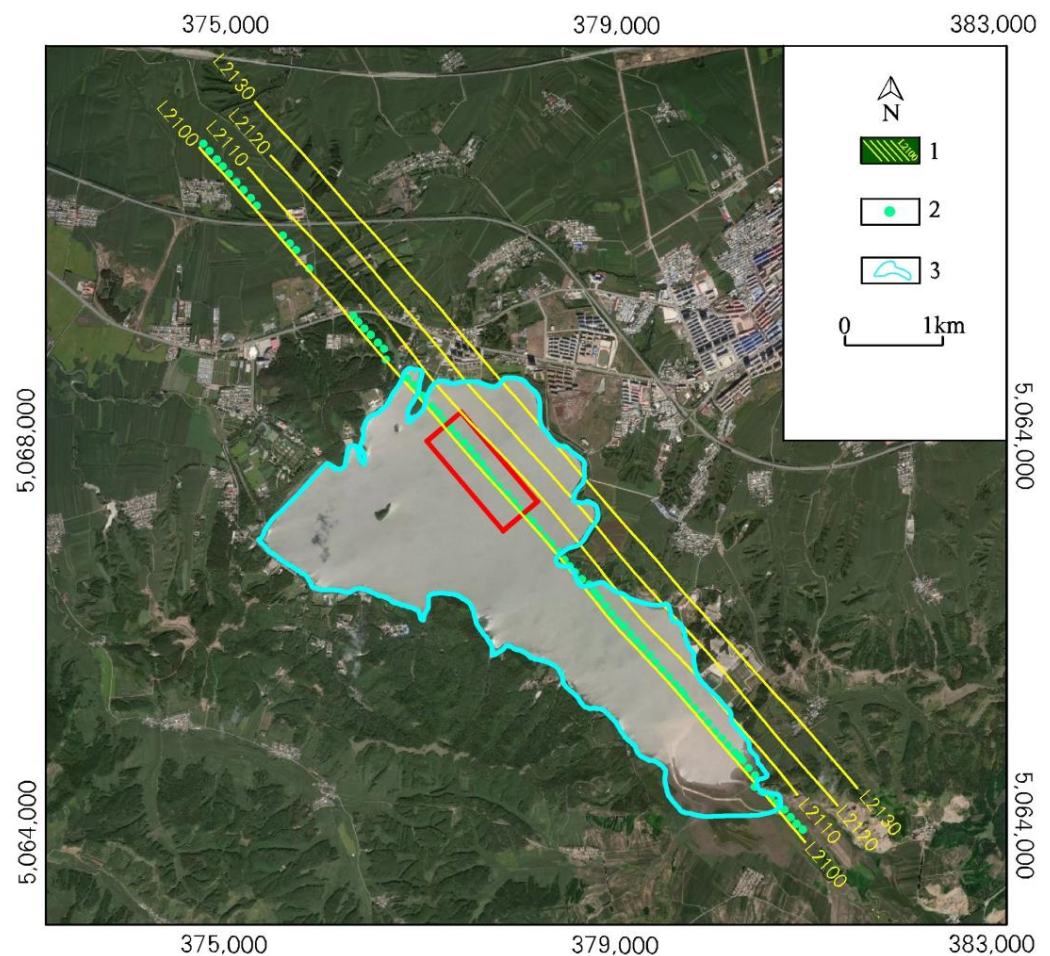


Figure 10. Ground TEM survey diagram. 1—flown footprint, 2—ground TEM survey position, 3—reservoir.

The transmitter was turned off, and data continued to be collected during the ground TEM measurement. The result of this measurement was the noise of the system in the

measurement area. In this way, the noise level maximum was 10 nT/s in early sampling channels and below 2 nT/s in middle and late sampling channels, as shown in Figure 11.

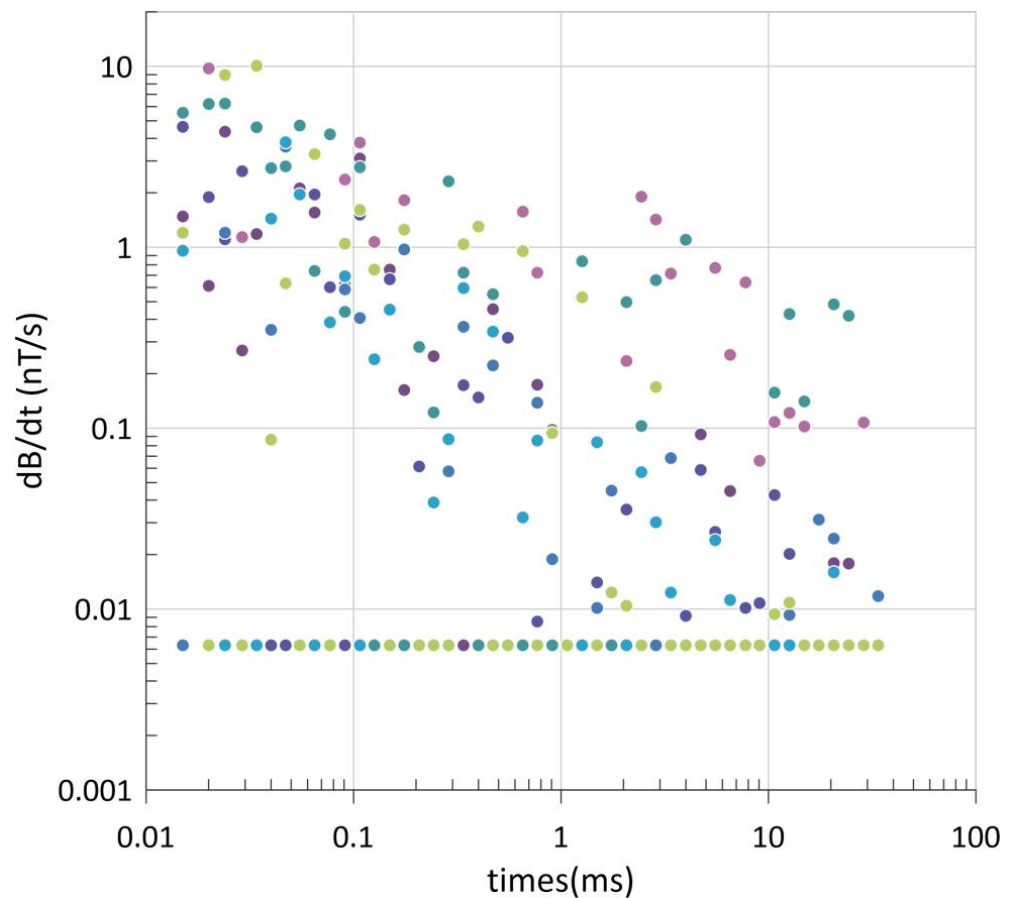


Figure 11. The noise level scatter diagram ground TEM measurement.

5. Results Comparison

The comparison between the L2100 profile response curves of iFTEM-I and TEM-30B is displayed in Figure 12. First, the amplitude of response from TEM-30B is 1 to 2 orders of magnitude larger than that from iFTEM-I, which is related to the measurement methods, device parameters, and mostly the flight altitude. Secondly, ground TEM measurement is easily affected by the interference of cultural buildings, so it was difficult to complete continuous measurements on the line. However, the general trends of the two measurements are basically consistent; the NW side of the survey line has a strong response, corresponding to the clay, loam, sandstone, and mudstone. The SE side's response is weak, corresponding to granite.

The inversion of TEM-30B data was completed using the one-dimensional inversion method with constraints [33]. In this article, the air and ground TEM data were inverted and compared by focusing on the lake area with less electromagnetic interference (the areas selected are shown in the red box and red dotted line in Figures 10 and 12). According to the inversion results (Figure 13), although the resistivity inversion values of the aerial data are lower, being about 75 m shallower and 250 m deeper, the two sets of data displayed consistency in the stratification of apparent resistivity depth. After comparison, we estimated that iFTEM-I can reach a prospecting depth of 300 to 350 m. Unfortunately, there was no drilling data or other information available to verify this more accurately.

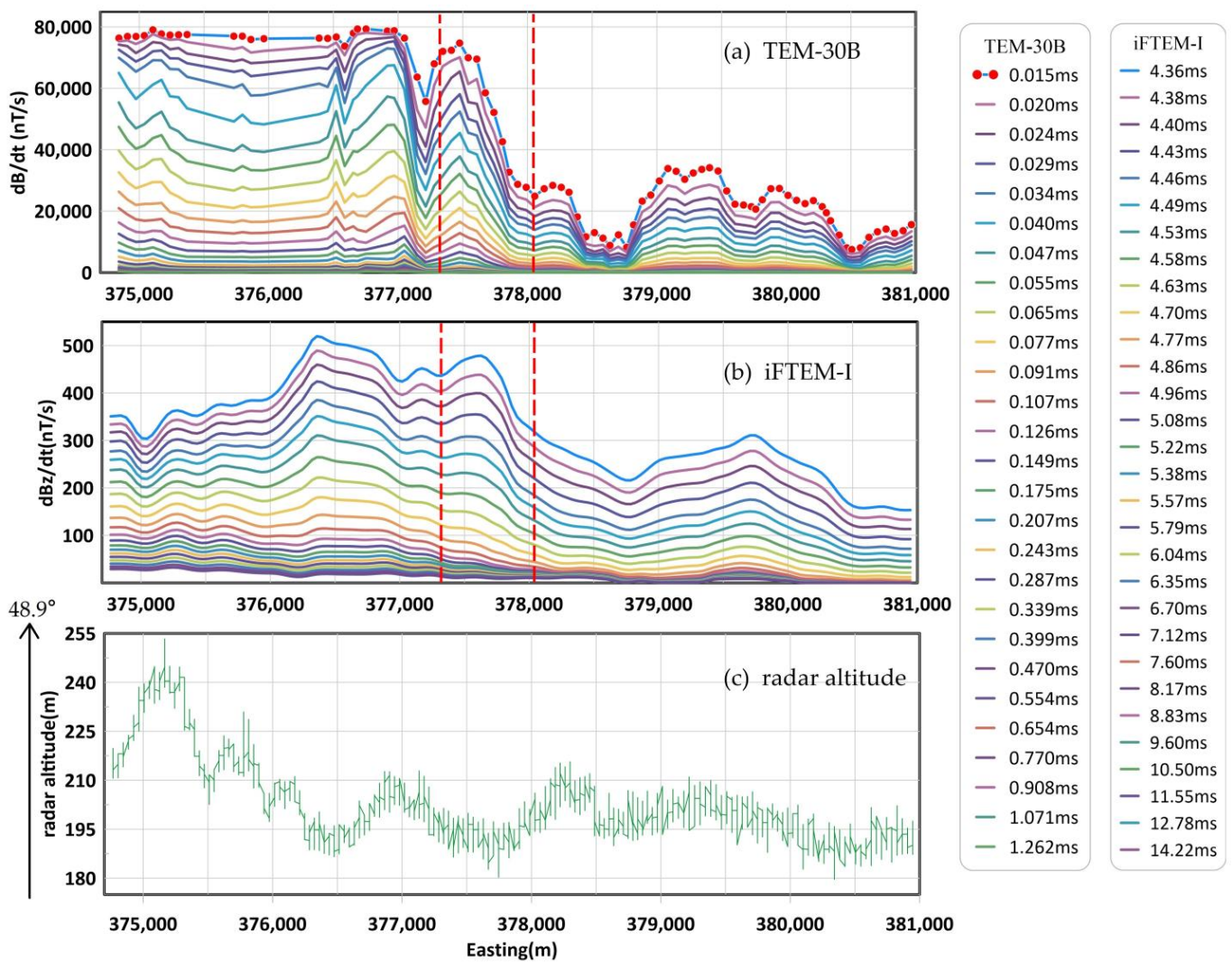


Figure 12. Comparison of profile response of L2100 between iFTEM and TEM-30B. (a) Profile response of TEM-30B (27 channels ahead); (b) profile response of iFTEM; (c) radar altitude of iFTEM. Between the red dash lines are the red rectangle areas from Figure 10.

The estimation of the depth of investigation for both TEM data is an important aspect of practical work. Skin depth (δ) is a very important concept in electromagnetic exploration; it is generally defined as the depth when the amplitude of the electromagnetic wave decays to $1/e$ of the ground amplitude in the propagation of underground medium [34].

$$\delta = \sqrt{\frac{2}{\sigma\mu_0\omega}} = \sqrt{\frac{2\rho T 10^7}{8\pi^2}} \approx 503\sqrt{\rho T} \tag{2}$$

where ρ is the average resistivity in the sample, and T is the time of gate center. According to Formula (2), we estimated the skin depth for both airborne and ground data and determined that the depth at the time of the system noise level was the max detection depth of the system in the sample. Finally, the range of investigation depth for airborne TEM data was over 190 m to 600 m at line 2100, and the range of investigation depth for ground TEM data was over 270 m to 700 m at line 2100.

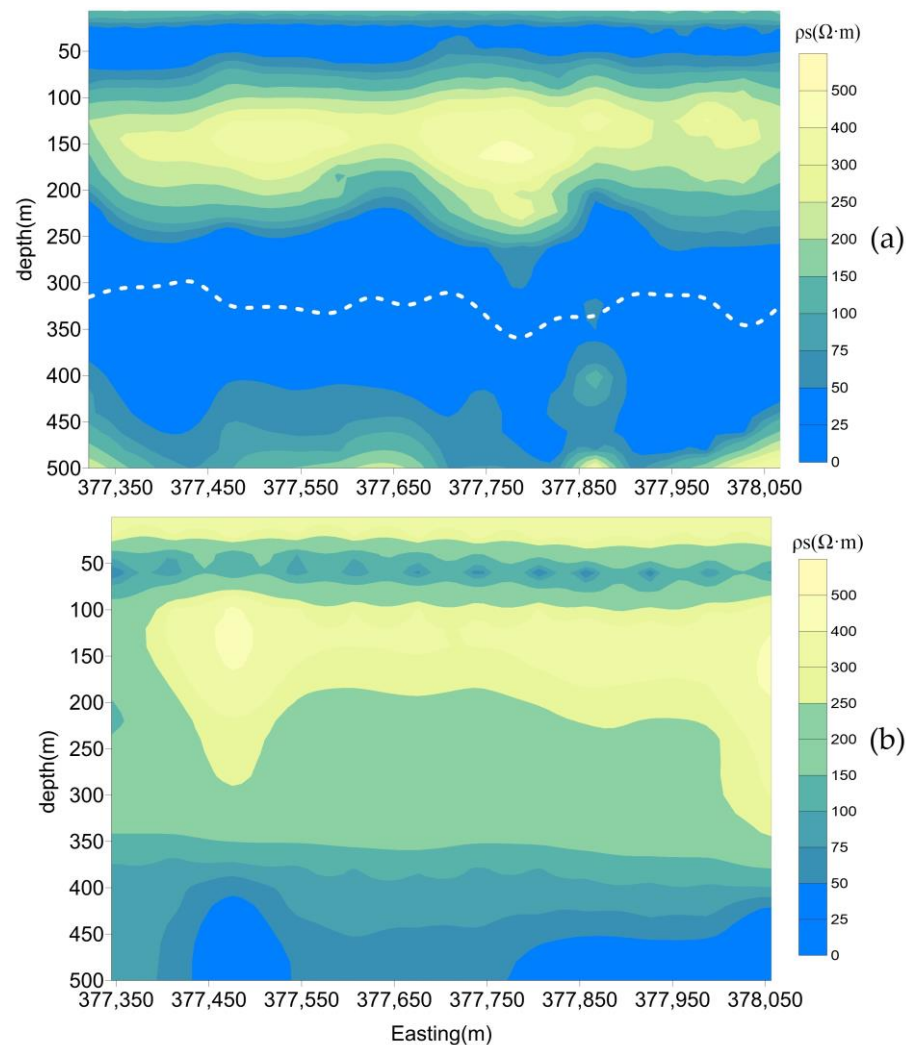


Figure 13. Comparison of inversion resistivity depth diagram between (a) iFTEM-I and (b) TEM-30B. The white dash line is the max depth of investigation according to Formula (2) and the peak-to-peak noise level (13 nT/s) in (a), not drawn in (b) because the maximum depth is deeper, and most are out of range.

6. Discussion

Y12-IV; aircraft's commercial load is 800 kg. The weight of the time-domain measurement system is about 410 kg. After the installation of iFTEM-I, the aircraft's single engine climb rate will reduce to 1 m/s, and the speed will also reduce to about 230 km/h or lower due to the increased wind resistance. Similarly, due to the increase in take-off weight, the flight time will reduce from 5.2 h to about 3.5 h. Considering these aspects, the system can only work in plains or areas with little topography at low and medium elevations, and the survey area should not be too far away from an airport. As a result, we were not able to select an area with better and more typical geological conditions for measurement.

Obviously, in the comparison with the ground time-domain transient electromagnetic method, we proved the validity of each of the method's measurements in low-interference areas. Additionally, it was shown that by using the fixed-wing time-domain airborne electromagnetic method, a line survey can be completed more quickly. Despite the lower influence of interference on the ground, it is possible to obtain more relatively complete geological information on the survey line. With the improvement of the system performance and signal noise ratio, the advantages of fixed-wing time-domain airborne electromagnetic method will be more noticeable.

7. Conclusions

In this article, we introduced the iFTEM-I system and verified the effectiveness of it by comparing airborne and ground TEM surveys. The successful development of the iFTEM-I system represents important progress in the R&D of the FTEM system of China, in which the goal of preliminary practical application has been reached and the technical gap in this field has been filled. Lots of important data were newly obtained in the survey flight in Binxian. The survey flight provided valuable experience for the subsequent improvement and practical application of the system.

Author Contributions: Conceptualization, J.L., N.L. and H.Z.; methodology, F.L., Q.M. and H.Z.; software, J.L., Q.Z., X.W. and H.Z.; validation, W.H. and Y.L.; investigation, J.L., N.L. and H.Z.; resources, F.L.; data curation, J.L., Q.Z. and H.Z.; writing—original draft preparation, H.Z. and N.L.; writing—review and editing, H.Z. and N.L.; visualization, H.Z.; project administration, H.Z. All authors have read and agreed to the published version of the manuscript.

Funding: This research was funded by the National Nonprofit Institute Research Grant of IGGE (No.AS2022J01 and No.AS2017J02) and the China Geological Survey (No.DD20190552).

Acknowledgments: The authors sincerely thank Xiaolan Feng's team for providing the TEM-30B instruments and corresponding technical support. The authors would also like to thank the anonymous reviewers and editors for their valuable suggestions.

Conflicts of Interest: The authors declare no conflict of interest.

References

1. Ping, H.; Wenjie, L.; Junfeng, L.; Qingmin, M.; Xuben, W.; Xiaodong, C.; Yingying, L. The Advances in the Development of Fixed-Wing Airborne Time-Domain Electromagnetic System. *Acta Geosci. Sin.* **2012**, *33*, 7–12. (In Chinese) [\[CrossRef\]](#)
2. Heath, P.; Dhu, T.; Keeping, T.; Reed, G.; Gouthas, G.; Katona, L.; Fairclough, M. A Review of AEM in South Australia. *ASEG Ext. Abstr.* **2013**, *2013*, 1–5. [\[CrossRef\]](#)
3. Fountain, D. Airborne Electromagnetic Systems—50 Years of Development. *Explor. Geophys.* **1998**, *29*, 11. [\[CrossRef\]](#)
4. Thomson, S.; Fountain, D.; Watts, T. Airborne Geophysics—Evolution and Revolution. 2007, pp. 19–37. Available online: <https://vdocuments.net/airborne-geophysics-evolution-and-exploration-against-this-background-of.html?page=1> (accessed on 24 April 2022).
5. Smith, R.; Fountain, D.; Allard, M. The MEGATEM Fixed-Wing Transient EM System Applied to Mineral Exploration: A Discovery Case History. *First Break* **2003**, *21*, 26–30. [\[CrossRef\]](#)
6. Reed, L.E. The Airborne Electromagnetic Discovery of the Detour Zinc-copper-silver Deposit, Northwestern Québec. *Geophysics* **1981**, *46*, 1278–1290. [\[CrossRef\]](#)
7. Leggatt, P.B.; Klinkert, P.S.; Hage, T.B. The Spectrem Airborne Electromagnetic System—Further Developments. *Geophysics* **2000**, *65*, 1976–1982. [\[CrossRef\]](#)
8. Lane, R.; Green, A.; Golding, C.; Owers, M.; Pik, P.; Plunkett, C.; Sattel, D.; Thorn, B. An Example of 3D Conductivity Mapping Using the TEMPEST Airborne Electromagnetic System. *Explor. Geophys.* **2000**, *31*, 162–172. [\[CrossRef\]](#)
9. Klinkert, P.S.; Leggatt, P.B.; Hage, T.B. The Spectrem Airborne Electromagnetic System—Latest Developments and Field Examples. *Proc. Explor.* **1997**, *97*, 557–564.
10. King, A.; Roux, T.L. Spectrem₂₀₀₀ AEM as a Mapping and Discovery System. *ASEG Ext. Abstr.* **2007**, *2007*, 1–3. [\[CrossRef\]](#)
11. Duncan, A.C.; Roberts, G.P.; Buselli, G.; Pik, J.P.; Williamson, D.R.; Roocke, P.A.; Thorn, R.G.; Anderson, A. SALTMAP—Airborne EM for the Environment. *Explor. Geophys.* **1992**, *23*, 123–126. [\[CrossRef\]](#)
12. Annan, A.P.; Lookwood, R. An Application of Airborne Geotem in Australian Conditions. *Explor. Geophys.* **1991**, *22*, 5–12. [\[CrossRef\]](#)
13. Changda, Z. Airborne Time Domain Electromagnetics System: Look Back and Ahead. *Chin. J. Eng. Geophys.* **2006**, *3*, 265–273. (In Chinese)
14. Yue, Z.; Feng, X.; Xiu, L. Review on Time-Domain AEM System and Applied Potential. *Prog. Geophys.* **2017**, *32*, 2709–2716. (In Chinese) [\[CrossRef\]](#)
15. Yin, C.-C.; Zhang, B.; Liu, Y.; Ren, X.; Qi, Y.-F.; Yifeng, P.; Qiu, C.; Huang, X.; Huang, W.; Jiajia, M.; et al. Review on Airborne EM Technology and Developments. *Chin. J. Geophys.* **2015**, *58*, 2637–2653. (In Chinese) [\[CrossRef\]](#)
16. Annan, A.P. Benefits Derived from the Use of a Fully Digital Transient Airborne EM System. In Proceedings of the SEG Technical Program Expanded Abstracts 1990, San Francisco, CA, USA, 23–27 September 1990; pp. 693–695.
17. Wynn, J. Evaluating Groundwater in Arid Lands Using Airborne Magnetic/EM Methods: An Example in the Southwestern U.S. and Northern Mexico. *Lead. Edge* **2002**, *21*, 62–64. [\[CrossRef\]](#)

18. Wolfgram, P.; Golden, H. Airborne EM Applied to Sulphide Nickel—Examples and Analysis. *ASEG Ext. Abstr.* **2001**, *34*, 136–140. [[CrossRef](#)]
19. Witherly, K.; Sattel, D. An Assessment of Geotem, Falcon[®] and ZTEM Surveys over the Nebo Babel Deposit, Western Australia. *ASEG Ext. Abstr.* **2018**, *2018*, 1–7. [[CrossRef](#)]
20. Witherly, K.; Diorio, P. Application of Airborne Magnetics, EM and Gravity to the Ring of Fire Intrusive Complex, Ontario. In Proceedings of the SEG Technical Program Expanded Abstracts 2014; Society of Exploration Geophysicists, Denver, Colorado, 5 August 2014; pp. 1704–1708.
21. Urbancich, J.; Wolfgram, P.; Sattel, D. AEM Bathymetry near Busselton, Western Australia—Comparison of 25 Hz and 12.5 Hz GEOTEM in Areas of High Conductance. *ASEG Ext. Abstr.* **2003**, *2003*, 1–4. [[CrossRef](#)]
22. Urbancich, J.; Macnae, J.; Sattel, D.; Wolfgram, P. A Case Study of AEM Bathymetry in Geographe Bay and over Cape Naturaliste, Western Australia, Part 2: 25 and 12.5 Hz GEOTEM. *Explor. Geophys.* **2005**, *36*, 381–392. [[CrossRef](#)]
23. Smith, R.S.; Koch, R.; Hodges, G.; Lemieux, J. A Comparison of Airborne Electromagnetic Data with Ground Resistivity Data over the Midwest Deposit in the Athabasca Basin. *Near Surf. Geophys.* **2011**, *9*, 319–330. [[CrossRef](#)]
24. Smith, R.S.; Koch, R. Airborne EM Measurements over the Shea Creek Uranium Prospect, Saskatchewan, Canada. In Proceedings of the SEG Technical Program Expanded Abstracts 2006; Society of Exploration Geophysicists: Houston, TX, USA, 2006; pp. 1263–1267.
25. Smith, R.S.; Cheng, L.Z.; Chouteau, M. Using Reversed Polarity Airborne Transient Electromagnetic Data to Map Tailings around Mine Sites. *Lead. Edge* **2008**, *27*, 1470–1478. [[CrossRef](#)]
26. Smith, R.S.; Annan, A.P.; Lemieux, J.; Pedersen, R.N. Application of a Modified GEOTEM System to Reconnaissance Exploration for Kimberlites in the Point Lake Area, NWT, Canada. *Geophysics* **1996**, *61*, 82–92. [[CrossRef](#)]
27. Paine, J.G.; Collins, E.W. *Applying Airborne Electromagnetic Induction in Ground-Water Salinization and Resource Studies, West*; Society of Exploration Geophysicists: Houston, TX, USA, 2003.
28. Dickinson, J.E.; Pool, D.R.; Groom, R.W.; Davis, L.J. Inference of Lithologic Distributions in an Alluvial Aquifer Using Airborne Transient Electromagnetic Surveys. *Geophysics* **2010**, *75*, WA149–WA161. [[CrossRef](#)]
29. Cheng, L.Z.; Smith, R.S.; Allard, M.; Keating, P.; Chouteau, M.; Lemieux, J.; Vallée, M.A.; Bois, D.; Fountain, D.K. Evaluation of the Efficiency of Several Airborne Electromagnetic Systems. *Explor. Min. Geol.* **2009**, *18*, 12.
30. Geotech Ltd. Evaluating Signal to Noise and Depth Investigation of Airborne Time. Available online: https://www.geotech.ca/documents/VTEM_SignaltoNoise.pdf (accessed on 3 April 2022).
31. Grant, F.S.; West, G.F. *Interpretation Theory in Applied Geophysics*; McGraw-Hill Book Co.: New York, NY, USA, 1965; ISBN 978-0070241008.
32. Zhili, X.; Wei, H.; Junjie, L.; Fei, L. Design and Implementation of Supporting Platform for Airborne Geophysical Exploration Software System. *Comput. Tech. Geophys. Geochem. Explor.* **2020**, *42*, 131–137. (In Chinese) [[CrossRef](#)]
33. Qingquan, Z.; Junjie, W.; Xiaohong, D.; Jie, Z. The One-Dimension Inversion of Underground Transient Electromagnetic Data. *Comput. Tech. Geophys. Geochem. Explor.* **2015**, *37*, 566–570. (In Chinese) [[CrossRef](#)]
34. Spies, B.R. Depth of Investigation in Electromagnetic Sounding Methods. *Geophysics* **1989**, *54*, 872–888. [[CrossRef](#)]